Adaptability of a data-driven fault detection and isolation approach

Fault Diagnosis in HVAC Chillers

Kihoon Choi,
Setu M. Namburu,
Mohammad S. Azam,
Jianhui Luo,
Krishna R. Pattipati, and
Ann Patterson-Hine

Modern buildings are being equipped with increasingly sophisticated power and control systems with substantial capabilities for monitoring and controlling the amenities. Operational problems associated with heating, ventilation, and air-conditioning (HVAC) systems plague many commercial buildings, often the result of degraded equipment, failed sensors, improper installation, poor maintenance, and improperly implemented controls.

Most existing HVAC fault-diagnostic schemes are based on analytical models and knowledge bases. These schemes are adequate for generic systems. However, real-world systems significantly differ from the generic ones and necessitate modifications of the models and/or customization of the standard knowledge bases, which can be labor intensive. Data-driven techniques for fault detection and isolation (FDI) have a close relationship with pattern recognition, wherein one seeks to categorize the input-output data into normal or faulty classes. Owing to the simplicity and adaptability, customization of a data-driven FDI approach does not require in-depth knowledge of the HVAC system. It enables the building system operators to improve energy efficiency and maintain the desired comfort level at a reduced cost.

In this article, we consider a data-driven approach for FDI of chillers in HVAC systems. To diagnose the faults of interest in the chiller, we employ multiway dynamic principal component analysis (MPCA), multiway partial least squares (MPLS), and support vector machines (SVMs). The simulation of a chiller under various fault conditions is conducted using a standard chiller simulator from the American Society of Heating, Refrigerating, and Air-Conditioning Engineers (ASHRAE) [1]. We validated our FDI scheme using experimental data obtained from different types of chiller faults.

This article first appeared in its original form at AUTOTESTCON 2004.

1094-6969/05/$20.00©2005IEEE

Description of the Target System

The target system of interest is the chiller of an HVAC system. The chiller is an HVAC component that produces chilled water for space-cooling purposes. The chiller system used in this article consists of a shell-and-tube evaporator, a shell-and tube condenser, a pilot-driven expansion valve, and a centrifugal compressor [2]. Figure 1 shows a centrifugal chiller and information flow diagram with sensor locations. An overview of the model and the faults experienced in a chiller, as well as the sensors available for its monitoring, are described next.

Model Description

Information flow within the system model and the various input-output variables for each component of a centrifugal chiller are presented in Figure 1. States 1, 2, 3, and 4 are the refrigerant states at the compressor inlet, condenser inlet, condenser outlet, and evaporator inlet, respectively. The following system dynamics are considered in the model [2]:

- refrigerant redistribution between the heat exchangers
- thermal capacitance of the tube material
- thermal capacitance of the water within the heat exchanger
- thermal capacitance of the valve's sensing bulb
- programmed dynamics of the compressors
- guide-vane controller.

In constructing the system model, the following assumptions were made [2]:

- Pressure drops in the heat exchangers and piping are negligible.
- Expansion across the valve and the cooling line orifice is isenthalpic.
- Compression is adiabatic.
- Two-phase regions in the heat exchanger are homogenous.
- Water-flow is single-pass in both heat exchangers.
- Tube material conductance is infinite.
- Shells are adiabatic.
- Water in each node is fully mixed.

The individual component models such as the heat exchangers, compressor, and valve are combined into a system model. The system states can be integrated forward in time, given an initial condition in terms of system pressures and

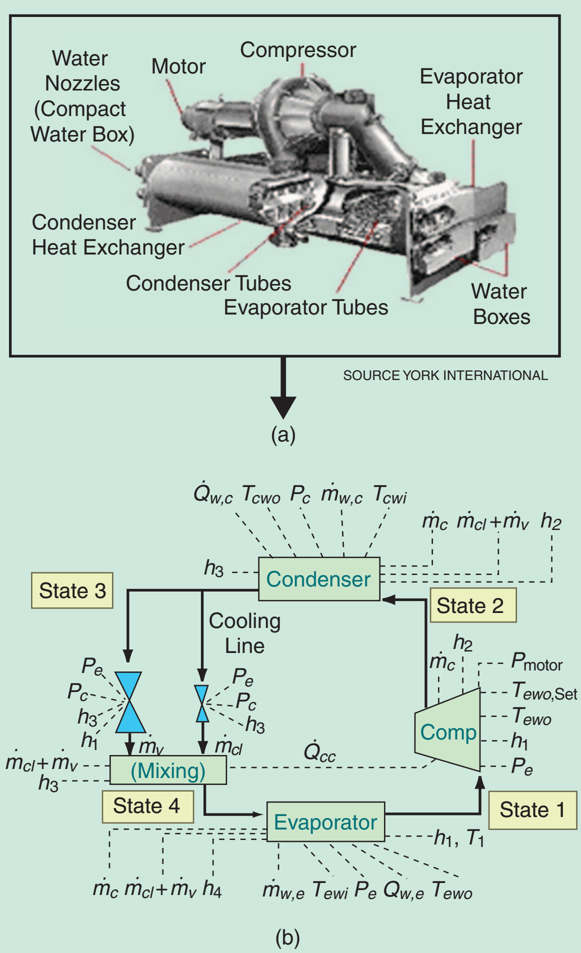

	Symbol	Description	Units
Input	T_{ewi}	Evaporator Water Entering Temperature	°C
	T_{cwi}	Condenser Water Entering Temperature	°C
	$T_{ewo,\mathrm{Set}}$	Chilled Water Set-Point Temperature	°C
	$\dot{m}_{w,e}$	Evaporator Water Mass Flow Rates	kg/s
	$\dot{m}_{w,c}$	Condenser Water Mass Flow Rates	kg/s
Output	P_e	Evaporator Pressure	kPa
	P_c	Condenser Pressure	kPa
	$\dot{Q}_{cc}$	Motor Heat Losses	kW
	P_{motor}	Motor Power	kW
	$\dot{Q}_{w,c}$	Condenser Water-Side Heat Rates	kW
	$\dot{Q}_{w,e}$	Evaporator Water-Side Heat Rates	kW
	T_{ewo}	Evaporator Leaving Water Temperature	°C
	T_{cwo}	Condenser Leaving Water Temperature	°C
	T_1	Refrigerant Temperature at Evaporator Exit	°C
	h_1	Refrigerant Enthalpy at Evaporator Exit	KJ/kg
	h_2	Refrigerant Enthalpy at Compressor Exit	KJ/kg
	h_3	Refrigerant Enthalpy at Condenser Exit	KJ/kg
	h_4	Refrigerant Enthalpy at Evaporator Inlet	KJ/kg
	$\dot{m}_c$	Refrigerant Flow Rate Through Com.	kg/s
	$\dot{m}_v$	Refrigerant Flow Rate Through Valve	kg/s
	$\dot{m}_{cl}$	Refrigerant Flow Rate Through Cooling Line	kg/s

(c)

Fig. 1. A centrifugal chiller and diagram of system model.

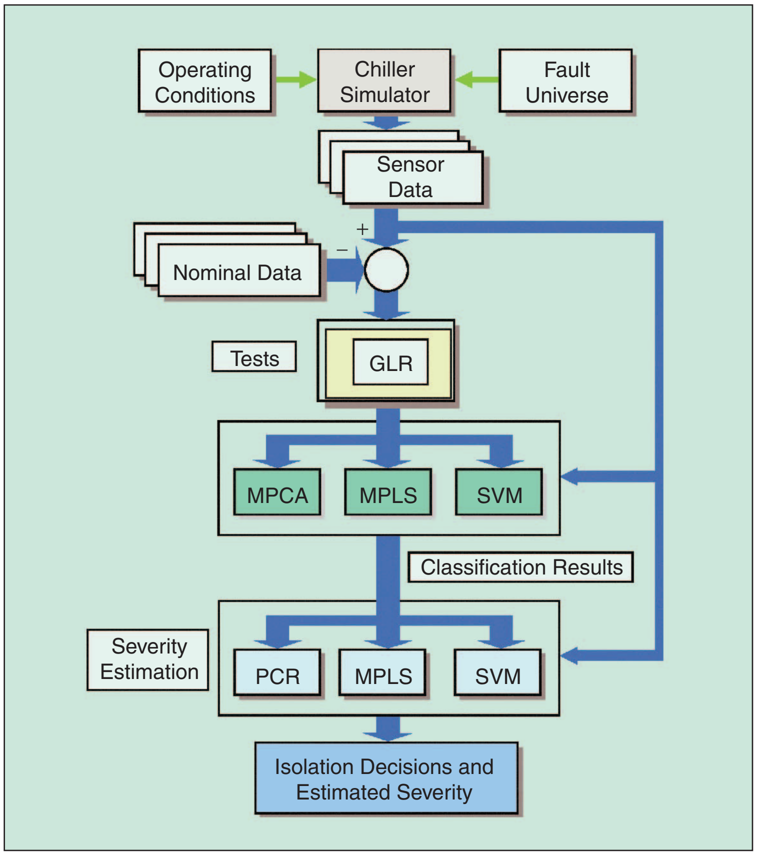

Fig. 2. Block diagram of real-time FDI scheme.

Diagnostic Process Overview

The block diagram of the real-time FDI scheme used in our approach is shown in Figure 2. We arranged the FDI scheme as a three-step process: fault detection, fault isolation using multivariate statistical techniques (MPCA and MPLS) and a neural network technique (SVM), and fault severity estimation using MPLS and SVM algorithms and principal component regression (PCR) [3].

For real-world systems, any monitored data is subjected to measurement noise. To simulate noisy data, we added Gaussian noise having zero mean and 0.5% of signal energy as variance. Usually, FDI of noisy data is much more challenging than the noiseless type. This is especially true in the case of a chiller, where the magnitudes of residuals are far smaller than those of the noise content. We observed that the low-frequency portion of the frequency spectra of the chiller data (from most of the sensors) contains all the variation information; hence, we employed a low-pass filter to reduce the noise content. The filter we employed is a windowed finite impulse response (FIR) filter with a pass band of 0–3 Hz. The FDI and severity estimation scheme for noisy data are illustrated in Figure 3.

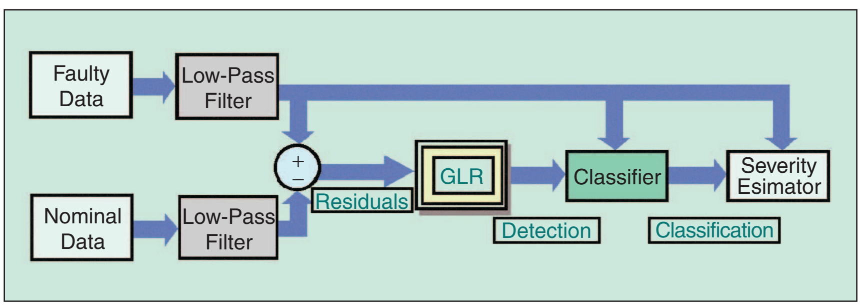

Fig. 3. FDI of noisy data.

Fault Detection

Fault detection is performed by monitoring the amount/rate deviation of a parameter from its nominal value. We employed a generalized likelihood ratio (GLR) test [4] for this purpose. The statistical test detects magnitude changes. We provide a short description of the test in the following section.

enthalpy distributions along the heat exchangers, inputs in terms of evaporator and condenser water temperatures (T_{ewi}, T_{cwi}), flow rates ($\dot{m}_{w,e}$, $\dot{m}_{w,c}$), and a chilled water set point temperature ($T_{ewo,\mathrm{Set}}$).

Fault Universe

The system is subject to five types of faults, including reduction in water flow rates in condenser (class 1) and evaporator (class 2), condenser and evaporator fouling (class 3 and class 4), and refrigerant undercharge (class 5).

Sensors

The system contains the following 28 sensors: one valve position, one valve flow area, two pressure, four flow-rate, four refrigerant enthalpy, four temperature, five mass, and seven heat power sensors.

GLR Test

In this article, we assume that the mean ω_o and variance σ^2 before the change are known, and the mean ω_1 after the change is unknown. For GLR, the log-likelihood ratio for the observations from time j up to time k is given by

$$R_j^k(\omega_1) = \sum_{i=j}^{k} \log \frac{P_{\omega_1}(r_i)}{P_{\omega_0}(r_i)}, \tag{1}$$

where $P_\omega(r_i)$ is the probability density function of the residual r at the time index i about the mean value ω. The ratio in (1) is a function of two unknown parameters: the change time and the value of mean after change. The standard statistical approach is to use the maximum likelihood estimates of these two parameters by

$$g_k = \max_{1 \le j \le k} \sup_{\omega_1} R_j^k(\omega_1). \tag{2}$$

We implemented the GLR test for a change in the mean, since the residual is found to be almost Gaussian under the normal conditions. Hence, the log-likelihood ratio in (1) simplifies to

$$R_j^k = \frac{\omega_1 - \omega_0}{\sigma^2} \sum_{i=j}^{k} \left(r_i - \frac{\omega_1 + \omega_0}{2} \right), \tag{3}$$

where σ^2 is the variance of the residual. Denoting $\eta = \omega_1 - \omega_0$, we obtain an estimate of η over the time window $[j, k]$ as

$$\hat{\eta}_j = \frac{1}{k - j + 1} \sum_{i=j}^{k} (r_i - \omega_0), \tag{4}$$

and the decision function in (2) becomes

$$g_k = \frac{1}{2\sigma^2} \max_{1 \le j \le k} \frac{1}{k - j + 1} \left[\sum_{i=j}^{k} (r_i - \omega_0) \right]^2. \tag{5}$$

Figure 4 shows a plot of the GLR test for the condenser pressure with 0.125% refrigerant undercharge and 0.28% condenser fouling. The straight line in the Figure 4(a) indicates the threshold for the nominal condition. We can clearly see that the GLR test detects the fault at $t = 0$ and even for very small severities.

Fault Isolation

The following techniques were used for fault isolation:

- MPCA [5], [6]
- MPLS [7], [8]
- Support vector machines (SVM) [9].

For ease of analysis, we arranged the experimental data in a three-dimensional array, $\underline{X}(I \times J \times K)$, as shown in Figure 5. Here, $\{j\}_1^J$ represent the sensors, $\{k\}_1^K$ are the time samples of the sensor readings, and $\{i\}_1^I$ are the batches of monitored data (normal and faulty cases).

MPCA

MPCA reduces the dimensionality of a data set and produces a representation in a manner that keeps the correlation structures among the process variables and is optimal in terms of capturing the variation in data.

MPCA decomposes the preprocessed data $\underline{X}_p$ in the following way:

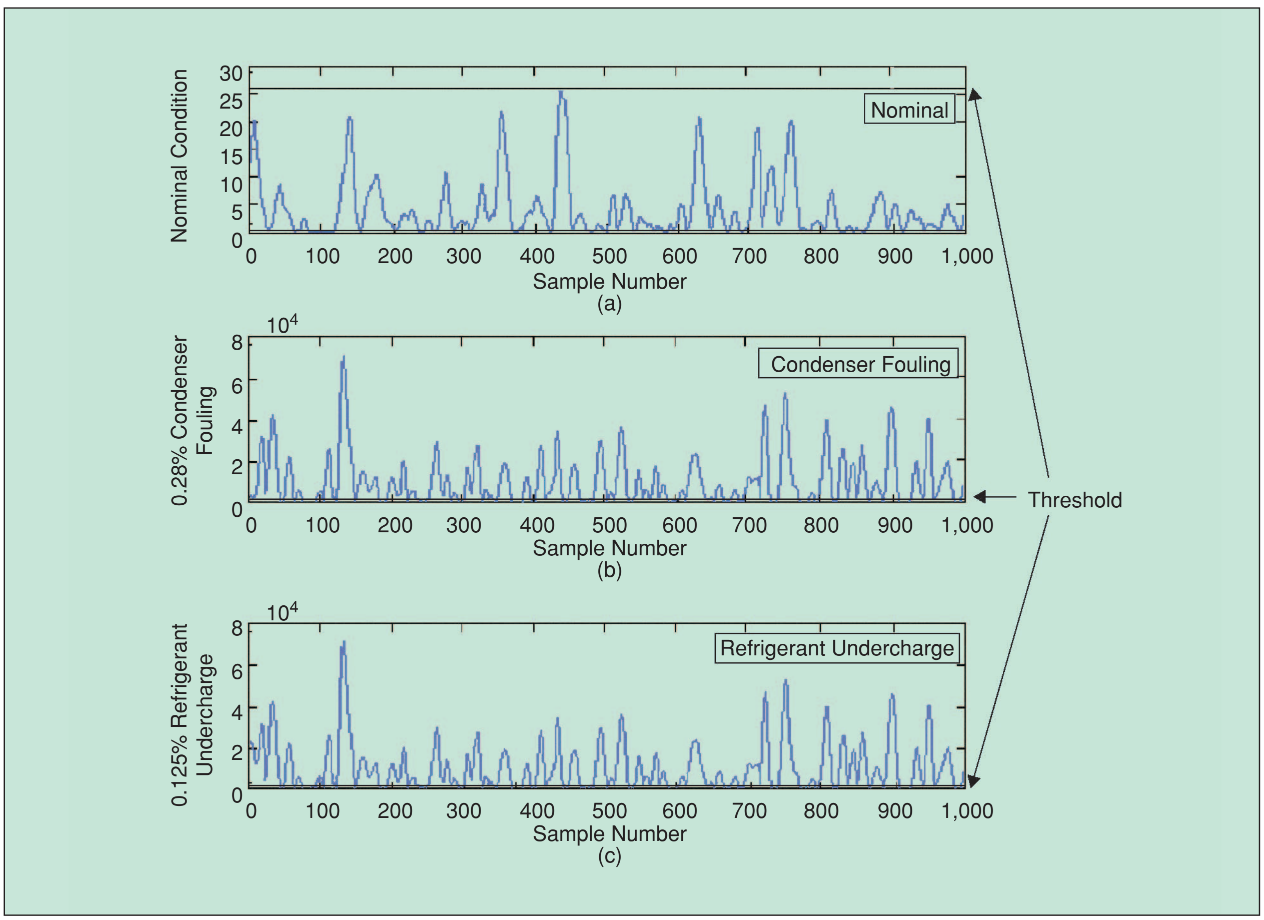

Fig. 4. GLR test for condenser pressure under normal and fault cases with different severities.

$$\underline{X}_p(i,j,k) = \sum_{a=1}^{L} t_a(i) P_a(k,j) + \underline{E}(i,j,k), \qquad (6)$$

where L is the number of principal components. A score vector t_a represents the relationship among I batches (each element of the score vector expresses the projection of the ith batch onto the reduced space), while P_a is a loading matrix that is related to the sensor readings (j) and their time variations (k). Loading matrices $\{P_a\}_{a=1}^{L}$ store all the structure information about how the sensor readings deviate from their mean values at each sample.

We used the nonlinear iterative partial least squares (NIPALS) algorithm for MPCA [10]. A preliminary classification of a new batch $\underline{X}_n (K \times J)$ can be tested for any unusual process behavior by obtaining its predicted t-scores and residuals [6]. The new scores, t_{test}, represent the projection of $\underline{X}_n$ onto the reduced L-dimensional space defined by the MPCA algorithm. If a new batch is similar to a specific class in the training data, the t_{test} scores will be located near the origin of the reduced space and the residual should be small. The distance of a new batch (test batch) from the origin of the reduced space can be measured by the following Hotelling statistic [6]:

$$D = t_{\text{test}} W t'_{\text{test}} I(I-L)/(L(I+1)(I-1)), \qquad (7)$$

where $W(L \times L)$ is the inverse covariance matrix of the t scores obtained from $\underline{X}$. If the t_{test} scores of a new batch are close to the origin, the batch can be easily isolated by defining the control limit for D via

$$D_{\text{lim}} = F_{L,I-L,\alpha}, \qquad (8)$$

where D_{lim} is the critical value of the F distribution at significance level α with L and $(I-L)$ degrees of freedom.

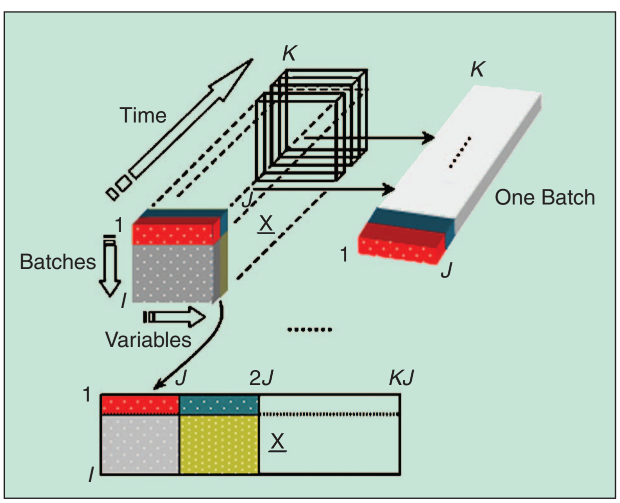

Fig. 5. Arrangement of a three-dimensional array for MPCA and MPLS.

MPLS

MPLS is a method for building regression models between the independent training data and the corresponding dependent variables (fault classes). The data array $\underline{X}$ in MPLS has the same form as that in MPCA, and for each $\mathbf{x}(K \times J) \in \underline{X}(I \times J \times K)$, there is a known set of response variables $\{y_{i,m}\} \in Y(I \times M)$ that represents the corresponding fault classes (M).

The goal of the MPLS algorithm is to make a decomposition of $\underline{X}$ into a set of triads. Each triad consists of one score vector t and two weight vectors w^J and w^K in the second and third dimensions, respectively. The model of $\underline{X}$ is given by

$$\underline{X}(i,j,k) = t_i \mathrm{w}_j^J \mathrm{w}_k^K. \qquad (9)$$

The MPLS model can be expressed as the problem of finding the vectors w^J and w^K that satisfy

$$\max_{\mathrm{w}^J \mathrm{w}^K} \left[\operatorname{cov}(t,y) \,\middle|\, \min \left(\sum_{i=1}^{I} \sum_{j=1}^{J} \sum_{k=1}^{K} \left(\underline{X}(i,j,k) - t_i \mathrm{w}_j^J \mathrm{w}_k^K \right)^2 \right) \right]. \qquad (10)$$

The least squares solution of (9) can be expressed as

$$\max_{\mathrm{w}^J \mathrm{w}^K} \left[\operatorname{cov}(t,y) \,\middle|\, t_i = \sum_{j=1}^{J} \sum_{k=1}^{K} \underline{X}(i,j,k) \mathrm{w}_j^J \mathrm{w}_k^K \right]. \qquad (11)$$

This implies

$$\max_{\mathrm{w}^J \mathrm{w}^K} \left[\sum_{i=1}^{I} t_i y_i \,\middle|\, t_i = \sum_{j=1}^{J} \sum_{k=1}^{K} \underline{X}(i,j,k) \mathrm{w}_j^J \mathrm{w}_k^K \right] = \max_{\mathrm{w}^J \mathrm{w}^K} \left[\sum_{j=1}^{J} \sum_{k=1}^{K} Z(j,k) \mathrm{w}_j^J \mathrm{w}_k^K \right]. \qquad (12)$$

The above can be maximized by formulating in terms of matrices as

$$\max_{\mathrm{w}^J \mathrm{w}^K} \left[(\mathrm{w}^J)^T Z \mathrm{w}^K \right] \Rightarrow (\mathrm{w}^J, \mathrm{w}^K) = \mathrm{SVD}(Z), \qquad (13)$$

where $\mathrm{SVD}(Z)$ means using the first set of normalized vectors from a singular value decomposition (SVD) on Z. The problem of finding w^J and w^K is simply accomplished by calculating this set of vectors [7].

SVM

The essential idea of SVM is to transform the signal to a higher-dimensional feature space and find an optimal hyperplane that maximizes the margin between the classes. We implemented a generalized form of SVM for overlapped and nonlinearly separable data. Briefly, the training data for the two classes are arranged as

$$F = [(x_1, y_1), (x_1, y_2), \ldots, (x_I, y_I)], \quad x_i \in R^{K \times J}, y_i \in \{-1, 1\}$$

$$\text{where } y_i = \begin{cases} 1, & \text{if } x_i \text{ belongs to the target class} \\ -1, & \text{otherwise.} \end{cases} \tag{14}$$

For the nonseparable case, a separating hyper-plane must satisfy the following constraints

$$y_i[\langle \mathrm{w}, \mathrm{x}_i \rangle + b] \geq 1 - \xi_i, \; i = 1, 2, \ldots, I, \tag{15}$$

where $\xi_i \geq 0$. To determine vectors w and b, the following function is minimized:

$$\Phi(w, \xi) = \frac{1}{2}\|w\|^2 + C\sum_{i=1}^{I}\xi_i \tag{16}$$

subject to the constraints in (15). The solution of (16) is given by the following dual optimization problem [11]:

$$\text{maximize } W(\alpha) = \sum_{i=1}^{I}\alpha_i - \frac{1}{2}\sum_{i=1}^{I}\sum_{j=1}^{I}\alpha_i\alpha_j y_i y_j \langle x_i, x_j \rangle,$$

$$\text{subject to}: \sum_{i=1}^{I}\alpha_i y_i = 0, \alpha_i \in [0, C], i = 1, 2, \ldots, I. \tag{17}$$

If a nonlinear mapping $K(x_i, x_j)$ is chosen a priori, the optimization problem of (17) becomes

$$\text{maximize } W(\alpha) = \sum_{i=1}^{I}\alpha_i - \frac{1}{2}\sum_{i=1}^{I}\sum_{j=1}^{I}\alpha_i\alpha_j y_i y_j K(x_i, x_j) \tag{18}$$

subject to the same set of constraints. The nonlinear mapping (or kernel function) K is used to transform the original input x to a higher-dimensional feature space Ω as $K(x_i, x_j) = \langle \phi(x_i), \phi(x_j) \rangle$, where $\langle .,. \rangle$ denotes the dot product. The decision function becomes

$$f(\mathrm{x}) = sgn\left(\sum_{i \in SVs}\alpha_i y_i K(x_i, x) + b\right). \tag{19}$$

where SVs is an index set that contains the index of the support vectors. In practice, various kernel functions are used, including polynomial, radial basis functions (RBF), and sigmoid functions. In this article, we use the RBF kernel functions

$$K(x_i, x_j) = \exp\left(-\|x_i - x_j\|^2 / 2\sigma^2\right). \tag{20}$$

Estimation of Fault Severity

Fault severity estimation is performed via MPLS and SVM algorithms and PCR. For the purpose of estimation, we train with the samples (training data) from one fault class using the associated severity levels as the targets (Y) (i.e., for each class, we train an individual estimator). Preclassified test samples are presented to the corresponding estimator and the estimated severity levels are obtained. The approach is shown in Figure 6.

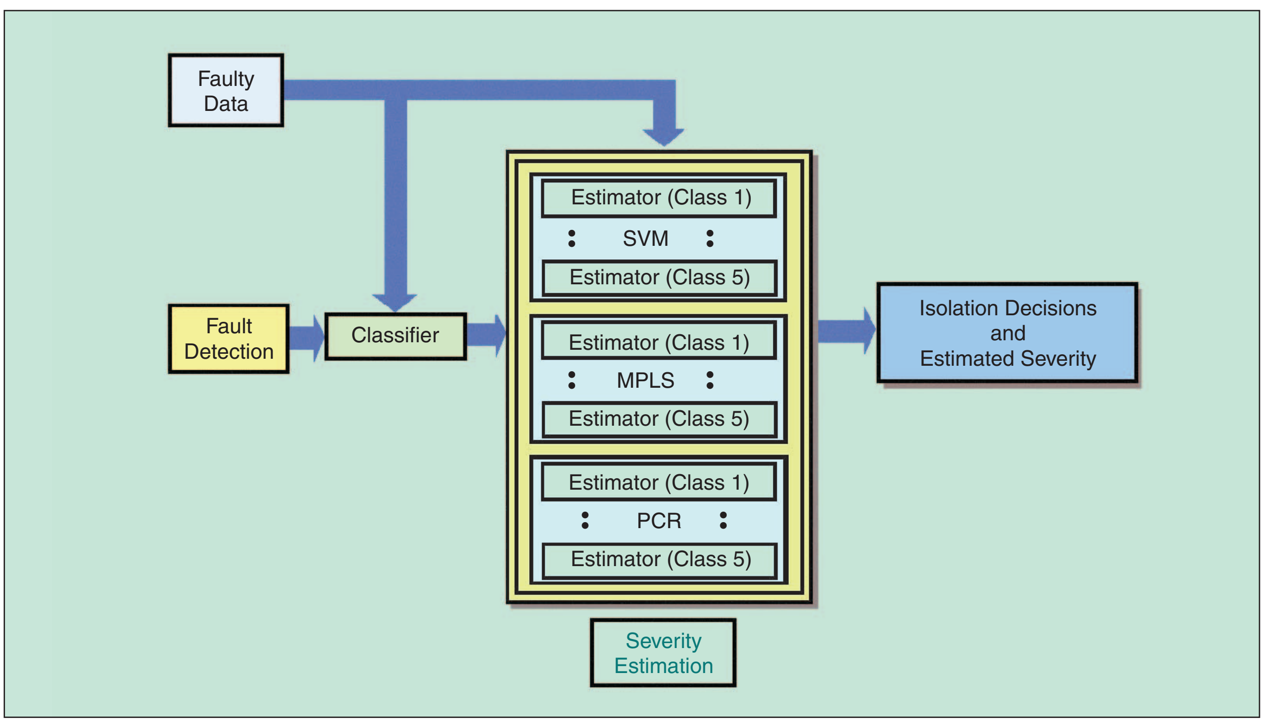

Fig. 6. Block diagram of estimation of fault severity by MPLS.

Simulation Results

The simulator provides observations for 28 sensor readings (variables). For each fault class, we performed simulations for 150 different severity levels; each run is sampled at 1,000 time points with a 1-s sampling interval. Classification and severity estimation results obtained via different techniques for noiseless and noisy data are given in the following sections. For MPCA and MPLS, the model reduction order was determined by cross validation [12]. We performed classification and fault severity estimation using SVM, MPCA, and PCR based on filtered data, while MPLS worked directly with noisy data because of its inherent filtering properties.

Data-driven techniques for fault detection and isolation (FDI) have a close relationship with pattern recognition, wherein one seeks to categorize the input-output data into normal or faulty classes.

Classification Results

For noiseless data, we found that the techniques provided more than 99% classification accuracy for all classes. The classification results of the three classifiers on noisy data are shown in Table 1.

Classification via MPCA

We trained the MPCA with half the collected data (i.e., 75 severity levels for each class) and tested on the rest. The classification results (using MPCA) in Table 1 were obtained with control limits of D (e.g., $D_{\text{lim}} = 3.29$) for each class. For noisy data, the number of false alarms increased. However, by means of further tuning the control limits of D, we avoided most of the false alarms.

Classification via MPLS

In this case, the training data $\underline{X}\,(375 \times 28 \times 1000)$ were centered (by subtracting from each column its mean) and then scaled via the double slab scaling method [13]. We found that the technique provided accurate classification for all classes, except for the nine false classifications for class 3 in the presence of noise.

Classification via SVM

For noiseless cases, the SVM parameters were $\sigma = 0.016$, $C = 1$, and $\xi = 0.001$. For noisy cases, we used $\sigma = 0.0000714$, $C = 100$, and $\xi = 0.001$. Among the techniques we employed for FDI of the chillers, SVM provides the most accurate classification. However, the performances of the other two classifiers are comparable to that of SVM.

Statistical Test

We performed McNemar's test [14] to compare the three techniques in terms of classification performance and found that the performance of SVM was better than MPCA and MPLS based on the chi-square statistic with one degree of freedom, e.g,

$$\text{MPCA} \underset{60\%}{\le} \text{MPLS} \underset{99.7\%}{\le} \text{SVM},$$

where $a \le b$ implies that technique b is better than (preferred to) technique a and % is the statistical confidence that technique b is better than technique a. It is evident that the

Table 1. Decision with noisy data.

True Class	Classifier	Class 1	Class 2	Class 3	Class 4	Class 5
Class 1	MPCA	71/75		4/75		
	MPLS	71/75		4/75		
	SVM	74/75		1/75		
Class 2	MPCA		74/75		1/75	
	MPLS		74/75	1/75		
	SVM		74/75		1/75	
Class 3	MPCA			75/75		
	MPLS			75/75		
	SVM			75/75		
Class 4	MPCA		13/75		62/75	
	MPLS			9/75	66/75	
	SVM				75/75	
Class 5	MPCA					75/75
	MPLS					75/75
	SVM					75/75

Table 2. Contingency tables for McNemar's test.

Classifier	MPLS	
SVM	15	1
	12	735
Classifier	**MPCA**	
SVM	20	0
	16	730
Classifier	**MPCA**	
MPLS	31	9
	14	719

performance of MPCA and MPLS are approximately the same, while the performance of SVM is significantly better than the other two. The contingency tables for the classifiers are shown in Table 2, where the (1,1) element denotes the number of times both classifiers are wrong; the (1,2) element is the number of times row classifier 1 is wrong but the column classifier is correct; the (2,1) element is the number of times the column classifier is wrong but the row classifier is correct; and the (2,2) element is when both classifiers are correct.

Table 3. Fault estimation results for noisy data.

Fault	True Value in %	MPLS Estimated Value in %	MPLS Avg. % of Error	PCR Estimated Value in %	PCR Avg. % of Error	SVM Estimated Value in %	SVM Avg. % of Error
Class 1	5.000	5.0043		5.1043		5.0347	
	21.50	21.574	0.78	21.521	0.66	21.461	0.44
	34.00	34.039		33.882		34.065	
Class 2	7.500	7.3626		6.999		7.5749	
	22.00	21.912	2.11	22.103	0.50	22.005	0.49
	39.50	39.621		39.764		39.442	
Class 3	13.44	11.780		13.197		12.494	
	15.68	15.476	4.45	15.439	11.02	15.994	4.32
	35.84	35.318		35.884		36.353	
Class 4	4.480	4.7787		5.9138		4.2530	
	28.56	28.394	1.89	27.165	5.47	28.395	1.48
	42.56	42.511		43.786		42.302	
Class 5	3.500	3.6556		3.4891		3.4704	
	12.25	12.391	1.31	12.231	0.343	12.224	0.434
	18.75	18.687		18.748		18.735	

Severity Estimation Results

The severity estimation results for noisy data are shown in Table 3. We randomly selected three different severities from each class and estimated those via MPLS, PCR, and SVM.

For noiseless cases, we found that for faults with severity levels above 10%, the error margins were below 1%. For faults with severity levels below 10%, the error margins never exceeded 10% of the true values.

The severity estimation results for noisy data are shown in Table 3. We randomly selected three different severities from each class and estimated those via MPLS, PCR, and SVM. Each average percent error in the table encompasses all the test patterns used for that class. It was evident that PCR was not as good as MPLS for fault severity estimation. SVM is slightly better than MPLS in terms of severity estimation performance and provides good estimation results for higher severity levels, although few error margins in the lower-severity levels exceeded 10% of the true values. However, MPLS and PCR are also comparable to the SVM performance for fault severity estimation.

Conclusions

In this article, a data-driven FDI scheme for the chillers in HVAC systems is presented. We employed the GLR test for fault detection and multivariate statistical techniques (MPCA and MPLS) and a neural network technique (SVM) for fault isolation. MPLS, SVM, and PCR were applied for fault severity estimation. The classification techniques provide accurate results, while the severity estimation process also precisely predicts the fault severity levels. The techniques are successfully applied to real chiller data provided by ASHRAE [15].

Our current approach deals with the entire time-series data. In the future, we plan to develop a generic FDI tool for chillers with an optimal sensor selection and employ signal processing (e.g., wavelet-based) techniques for feature extraction. The feature space, being far smaller than the original data, is expected to reduce the computation time and result in better diagnosis.

Acknowledgment

This work was supported by NASA-ARC under contract NAG-1635.

References

[1] American Society of Heating, Refrigerating and Air-Conditioning Engineers [Online]. Available: http://www. ashrae.org

[2] S. Bendapudi and J.E. Braun, "Development and validation of a mechanistic, dynamic model for a vapor compression centrifugal liquid chiller," Ray W. Herrick Labs., HL 2002-8, Purdue Univ., West Lafayette, IN.

[3] A. Smilde, R. Bro, and P. Geladi, *Multi-Way Analysis: Applications in the Chemical Sciences*. London: Wiley, 2004.

[4 M. Basseville and I.V. Nikiforov, *Detection of Abrupt Changes: Theory and Application* (Prentice-Hall Information and System Sciences Series). Englewood Cliffs, NJ: Prentice-Hall, 1993.

[5] P. Nomikos and J.F. MacGregor, "Monitoring batch processes using multiway principal component analysis," *Amer. Inst. Chem. Eng.*, vol. 40, no. 8, pp. 1361–1375, 1994.

[6] P. Nomikos, "Detection and diagnosis of abnormal batch operations based on multi-way principal component analysis," *ISA Trans.*, vol. 35, no. 3, pp. 259–266, 1996.

[7] B. Rasmus, "Multiway calibration. Multilinear PLS," *J. Chemometrics*, vol. 10, no. 1, pp. 47–61, 1996.

[8] C. Junghui and K.-C. Liu, "On-line batch process monitoring using dynamic PCA and dynamic PLS models," *Chem. Eng. Sci.*, vol. 57, no. 1, pp. 63–75, 2002.

[9] H. Chih-Wei and C.-J. Lin, "A comparison of methods for multi-class support vector machines," *IEEE Tran. Neural Networks*, vol. 13, no. 2, pp. 415–425, Mar. 2002.

[10] S. Wold, P. Geladi, K. Esbensen, and J. Ohman, "Principal component analysis," *Chemometrics Intell. Lab. Syst.*, vol. 2, no. 1–3, pp. 37–52, 1987.

[11] M. Ge, R. Du, G. Zhang, and Y. Xu, "Fault diagnosis using support vector machine with an application in sheet metal stamping operations," *Mech. Syst. Signal Processing*, vol. 18, no. 1, pp. 143–159, 2004.

[12] J.E. Jackson, *A User's Guide to Principal Components*. New York: Wiley, 1991.

[13] P.S. Gurden, J.A. Westerhuis, B. Rasmus, and A.K. Smilde, "A comparison of multiway regression and scaling methods," *Chemometrics Intell. Lab. Syst.*, vol. 59, no. 1–2, pp. 121–136, 2001.

[14] E. Alpaydin, *Introduction to Machine Learning*. Cambridge, MA: The MIT Press, 2004.

[15] M. Namburu, M. Azam, J. Luo, K. Choi, and K.R. Pattipati, "Fault detection, diagnosis and data-driven modeling in HVAC chillers," in *Proc. SPIE Conf.*, Orlando, FL, Mar. 2005.

Kihoon Choi received the B.Sc. degree in electrical and electronic engineering in Korea in 2000. Currently, he is pursuing his Ph.D. at the University of Connecticut. His research interests are in the areas of fault diagnosis of complex systems, system real-time fault diagnosis, and analysis and optimization of large-scale systems.

Setu M. Namburu completed her B.Tech. degree in electrical and electronics engineering in India and entered the Electrical and Computer Engineering Department at the University of Connecticut as a Master's student in 2003. Her research interests include systems analysis, automation, and fault diagnosis.

Mohammad S. Azam received the B.Sc. degree in electrical and electronic engineering from Bangladesh University of Engineering and Technology, Dhaka, in 1997, and the M.S. degree in control and communication systems engineering from the University of Connecticut in 2002. Currently, he is pursuing his Ph.D. in the same department. His research interests include diagnosis of power quality events, fault diagnosis in large systems, reliability analysis, and analysis and optimization of large-scale systems.

Jianhui Luo is a graduate student in the Electrical and Computer Engineering Department at the University of Connecticut. Previously, he was at Shanghai Institute of Railway Technology, China, from which he received his B.A.Sc. in automatic control in 1993. He worked as a design engineer and later as deputy department head at CASCO Signal Inc. in Shanghai, China, from 1993–2000. His primary research interests include system simulation, model-based system fault diagnosis, and safety critical system analysis.

Krishna R. Pattipati (krishna@engr.uconn.edu) is a professor of electrical and computer engineering at the University of Connecticut, Storrs. He has published over 300 articles, primarily in the application of systems theory and optimization techniques to large-scale systems. He received the Centennial Key to the Future award in 1984 from the IEEE Systems, Man, and Cybernetics Society. He received the Andrew P. Sage award for the Best IEEE Systems, Man, and Cybernetics Society Transactions Paper for 1999, the Barry Carlton award for the Best Aerospace and Electronic Systems Society Transactions Paper for 2000, the 2002 NASA Space Act Award, and the 2003 AAUP Research Excellence Award at the University of Connecticut. He also received the best technical paper awards at the 1985, 1990, 1994, 2002, and 2004 IEEE AUTOTESTCON, as well as at the 1997 and 2004 Command and Control Conferences. He was editor-in-chief of *IEEE Transactions on SMC-Cybernetics (Part B)* from 1998–2001. He is a Fellow of the IEEE.

Ann Patterson-Hine received the Ph.D., P.E., in mechanical engineering from the University of Texas at Austin in 1988. She has worked at Ames Research Center since July 1988, where she is group leader of the Research in Intelligent Vehicle Automation Group in the Computational Sciences Division at NASA Ames Research Center. She has been the project leader for advanced technology demonstrations under the Next Generation Launch Technology Program and many of the program's predecessors. She participated in the Shuttle Independent Assessment Team and Wire Integrity Pilot Study at Ames. Her research has centered on the use of engineering models for model-based reasoning in advanced monitoring and diagnostic systems.